horticulturae

MDPI

Article

Design and Ventilation Optimization of a Mechanized Corridor in a Solar Greenhouse Cluster

Ming He [1,2,3], Xinxia Jiang [1,2,3], Xiuchao Wan [1,2,3], Yiming Li [2,3,4], Qinglu Fan [5,*] and Xingan Liu [1,2,3]

1 College of Horticulture, Shenyang Agricultural University, Shenyang 110866, China; mhe23@syau.edu.cn (M.H.); 13066697003@163.com (X.J.); ljy990205@outlook.com (X.W.); lxa10157@syau.edu.cn (X.L.)
2 Key Laboratory of Protected Horticulture, Shenyang Agricultural University, Ministry of Education, Shenyang 110866, China; liyiming@syau.edu.cn
3 National & Local Joint Engineering Research Center of Northern Horticultural Facilities Design & Application Technology (Liaoning), Shenyang 110866, China
4 College of Engineering, Shenyang Agricultural University, Shenyang 110866, China
5 Xinjiang Academy of Agricultural and Reclamation Sciences, Shihezi 832000, China
* Correspondence: maymajy@163.com

Abstract: Corridors play an important role in the mechanized production of fruits and vegetables in solar greenhouse clusters. A corridor structure that is suitable for the automated production of solar greenhouse clusters is designed in this paper. To increase the corridor's ventilation efficiency and enhance the temperature environment, the computational fluid dynamics method is applied to analyze the effects of corridor structure, ventilation mode, wind speed, and direction on internal temperature and humidity. Studies have indicated that an erroneous layout of the corridor structure may result in the formation of accumulated temperature and heat concentration inside, and ventilation within the corridor is essential. The corridor's ideal dimensions are 3.2 m high by 5 m wide, and it has an internal wind speed and cooling rate that are superior to other structural factors. The ventilation method adopts a combination of top and bottom ventilation, and when the bottom window opening is 70%, there is a good ventilation effect inside the corridor. The corridor has an excellent ventilation effect when the wind speed is 2 m/s and the wind direction is east or west. This study supports the intensive and sustainable growth of greenhouse vegetable production by providing guidance for the planning and corridor design of solar greenhouse clusters.

Keywords: solar greenhouse cluster; mechanized corridor; combined ventilation; accumulated temperature; flow field

Citation: He, M.; Jiang, X.; Wan, X.; Li, Y.; Fan, Q.; Liu, X. Design and Ventilation Optimization of a Mechanized Corridor in a Solar Greenhouse Cluster. *Horticulturae* **2024**, *10*, 1240. https://doi.org/10.3390/horticulturae10121240

Academic Editor: Nazim S. Gruda

Received: 2 November 2024
Revised: 20 November 2024
Accepted: 20 November 2024
Published: 22 November 2024

1. Introduction

In modern architecture, a corridor is an overhead connection that meets both functional and aesthetic requirements for two or more high-rise buildings. Corridors are also used in agricultural production. Crops cannot be grown in open fields in northern China due to the harsh winters. In these areas, annual fruit and vegetable production is possible thanks to solar greenhouses [1]. Chinese solar greenhouses typically include a transparent front roof, a back roof, a back wall, and two side walls. The transparent front roof can generate the greenhouse effect, while the back wall can store excess energy during the day and release it at night. Through these principles, Chinese solar greenhouses greatly reduce energy input. However, the cold weather greatly reduces the connectivity of greenhouses. The issue of poor greenhouse connectivity can be effectively resolved and the integration of production, transportation, and management of solar greenhouse clusters can be facilitated using corridors to connect multiple solar greenhouses in series [2]. Typically, corridors use transparent glass or plastic film as the covering material, which results in concentrated and uneven temperature under sunlight [3], which is not conducive to the work of production

personnel. Therefore, it is essential to appropriately plan the corridor's structure and enhance its ventilation capabilities for the intended use [4–6].

Since most existing solar greenhouses are standalone structures, it is impossible to load or unload fruits or seedlings when it is raining or snowing outside. At the same time, summer and winter temperature extremes negatively impact the quality of fruits and seedlings [7–9]. The corridor design of the solar greenhouse cluster can not only solve the above problems but also facilitate small mechanical cross-shed operations such as tillage, spraying, picking, transportation, etc. Additionally, the corridor can act as a plastic greenhouse for drying and other agricultural product processing [10–13]. The solar greenhouse industry benefits from the corridor as well. To improve the production process's characteristics related to the service industry, crop displays can be arranged like a conventional urban health facility [14]. By showing a variety of plant species on both sides of the corridor, people will be better able to comprehend the kinds of plants grown in greenhouses and the conditions under which they thrive, giving the greenhouse an educational purpose [15]. Mechanized corridors, which connect greenhouses, crop displays, rest, and communication areas, are a crucial component of modern solar greenhouse clusters. They facilitate efficient and convenient operation and management of greenhouse clusters.

Due to the similarity in principle and form between corridors and plastic greenhouses, ventilation must be fully considered in the design. However, as an innovative greenhouse facility, the corridor still lacks extensive discussion among scholars. Numerous academics have studied greenhouse ventilation techniques, concentrating on ways to increase greenhouse ventilation effectiveness. He et al. [16] employed computational fluid dynamics (CFDs) numerical simulations to investigate the impact of various vent sizes on the thermal environment of greenhouses, and a ventilation strategy for detachable north walls was proposed. This technique lowered the greenhouse's maximum temperature by approximately 5.8 °C and its average temperature by about 1.7 °C when compared to a con-venational brick wall solar greenhouse. The effects of environmental factors on the thermal environment of strawberry greenhouses with natural ventilation, including the air inlet size, outside temperature, and ambient wind speed, were examined and summarized by Fu and You [17]. Zhang et al. [18] examined the connection between ventilation and humidity in Chinese solar greenhouses (CSGs) using a combination of the energy balance model and the CFDs model. It was discovered that while the temperature and humidity of CSGs decrease and exhibit a non-linear change process, the natural ventilation volume increases as ventilation openings increase. Through experiments and numerical simulations, Li et al. [19] designed a ventilation scheme for a circular arched solar greenhouse and investigated the greenhouse's cooling and ventilation effects. Three ventilation structures were compared in terms of performance by Zhang et al. [20]: front bottom + top (FT), front bot-tom + back roof (FB), and front bottom + top + back roof (FTB). Upon comparing FTB to FT and FB, the cooling rate increased by 24.84% and 5.52%, respectively, while the average temperature dropped by 13.81% and 3.65%, respectively.

Corridor structures cannot, however, be directly affected by the findings of research on the ventilation in solar greenhouses. The way a corridor is built affects the entire greenhouse cluster and cannot be compared to the variations in humidity and temperature in a single solar greenhouse. As a result, studies on corridors should be conducted on a larger scale, comparable to that of building clusters in the construction sector, and cover the entire park [21]. Both the external wind field size of the 3D model [22] and the choice of research variables to simplify the model [23] are areas of extensive and well-developed experience. Moreover, corridors play an important role in the intensive production of greenhouses. Attempting to construct low-cost corridors and adopting natural ventilation can serve as a more sustainable and resource-saving method for promoting greenhouse vegetable cultivation [24].

To sum up, corridors are an essential component of solar greenhouse cluster modernization. However, research on the use of corridors for facility agriculture production is scarce, as are studies on the most effective methods for maximizing corridor ventilation.

Consequently, a mechanized corridor structure for solar greenhouse clusters is developed in this paper, and the temperature concentration phenomenon caused by the corridor structure is quantitatively explained. Then, in order to maximize the ventilation effect of the corridor, the effects of various factors are examined separately, including the corridor structure parameters, ventilation techniques, wind direction, and speed. This study can provide theoretical guidance for the corridor design of solar greenhouse clusters.

2. Numerical Simulation

2.1. Geometric Model

As seen in Figure 1, the solar greenhouse cluster was made up of eight identical energy-saving solar greenhouses. The dimensions of every solar greenhouse were 12 m in width, 60 m in length, and 6 m in height. The greenhouse's ventilation system was a combination of bottom and top ventilation, with two 60 m by 1 m ventilation openings. The greenhouses were joined by the mechanized corridor. The separation between neighboring greenhouses was 15 m in the east and 9 m in the south. The corridor was 72.5 m long in the north–south direction, with a height of h (3.2, 3.7, 4.2, 4.7, 5.2 m) and a width of w (4, 5, 6, 7 m). The two ways the corridor was ventilated were the top and bottom ventilation. The top window had a width of 0.5 m and a length of 72.5 m. The bottom window had various bottom ventilation openings η (10%, 30%, 50%, 70%, and 90%) set, and it measured 1 m wide by 72.5 m long from the ground.

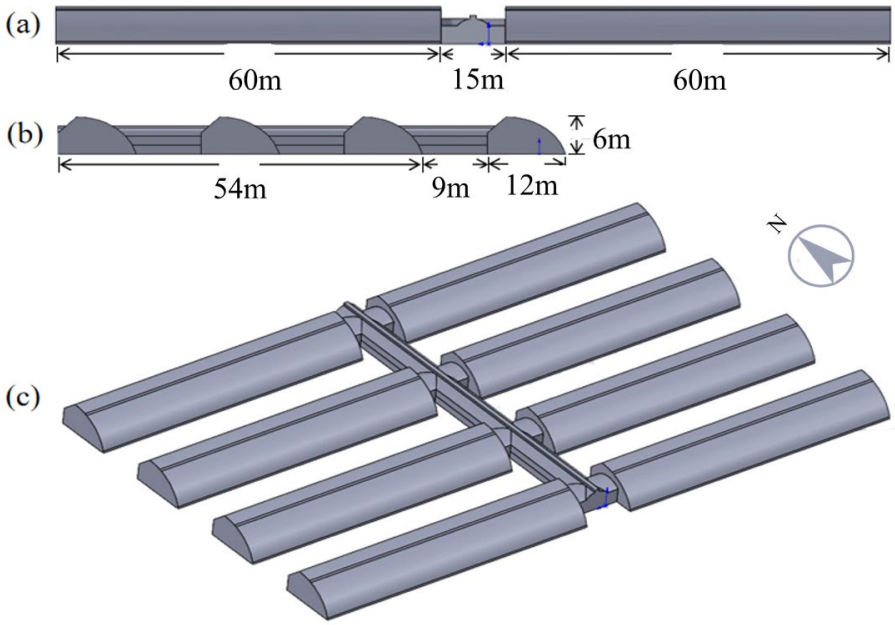

Figure 1. Geometric models of the greenhouse cluster and corridor: (**a**) Front view; (**b**) Side view; (**c**) Overall picture.

The greenhouse and corridor's mesh details are displayed in Figure 2a. The accuracy of the simulation results varies depending on the mesh quantity [25]. Temperature was used to confirm the convergence of simulations with various mesh quantities. The results remained stable when the mesh quantity reached 2.45×10^4 (Figure 2b). The grid quality is shown in Figure 2c. To ensure the accuracy of simulation calculations, this study selected a mesh model of this size. Using three different time steps of 1 s, 5 s, and 10 s, the temperatures were almost the same. A maximum acceptable time step of 10 s was selected, considering the computational cost. The hexahedral mesh was used to divide the model, and local meshes were refined to increase the computational accuracy so that the mesh distortion was less than 0.7 [26].

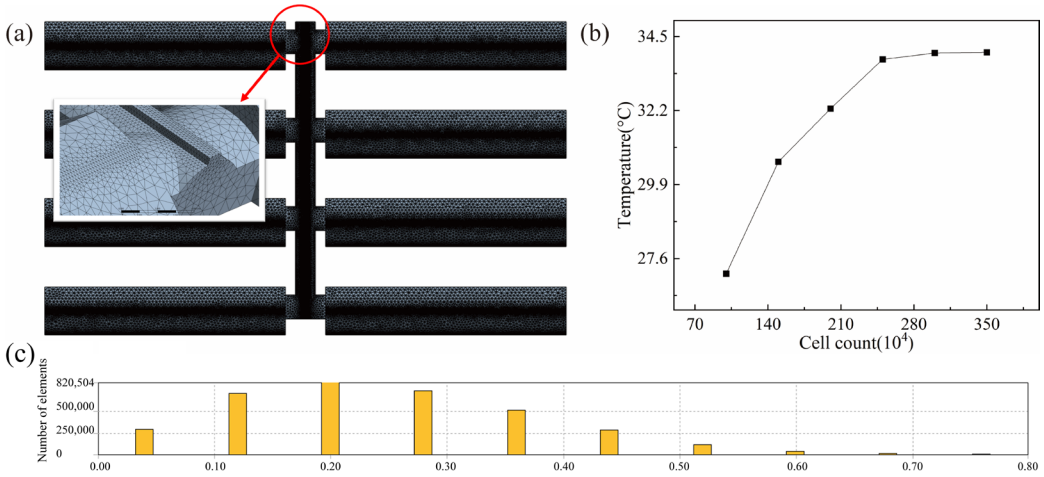

Figure 2. Mesh: (**a**) Mesh details; (**b**) Correlation analysis; (**c**) Skewness quality.

2.2. Mathematical Model

The air flow in solar greenhouses and corridor follows the conservation equations of mass, momentum, and energy [27]. The finite element discretization method was primarily used in conjunction with them to analyze the fluid flow. Simplifying the analyzed model and reducing the calculation steps allowed for an effective analysis of air flow field.

$$\frac{\partial \rho}{\partial t} + \mathrm{div}(\rho \vec{v}) = S_\mathrm{m} \tag{1}$$

$$\frac{\partial}{\partial t}(\rho \vec{v}) + \mathrm{div}(\rho \vec{v}\vec{v}) = \mathrm{div}[\mu(\mathrm{div}\vec{v})] - \mathrm{div}P + \rho \vec{g} + \vec{F} + S \tag{2}$$

$$\frac{\partial}{\partial t}(\rho T) + \mathrm{div}(\rho \vec{v} T) = \mathrm{div}\left(\frac{\tau}{c}\mathrm{grad}T\right) + S_\mathrm{T} \tag{3}$$

where S_m represents the mass added to the continuous phase, kg; $\vec{v}$ represents the speed, m/s; t is time, s; and ρ represents the density, kg/m^3. $\vec{F}$ is the volume force, Pa; μ is the viscosity, Pa·s; P is the pressure, Pa; $\vec{g}$ is the gravitational acceleration, m/s^2; S is the momentum source term; T is the temperature, °C; τ is the heat transfer coefficient, W/(m^2·°C); c is the specific heat capacity, J/(kg·°C); and S_T is the viscous dissipation term.

Due to the constant presence of turbulence in the corridor, different turbulence models have entirely different effects on the simulated temperature and flow fields. After comparing various turbulence models (RNG k-ε, Standard k-ε, and Realizable k-ε), this study's simulation calculations used the Realizable k-ε model [28].

$$\frac{\partial(\rho k)}{\partial \mathrm{t}} + \frac{\partial(\rho k u_i)}{\partial x_i} = \frac{\partial}{\partial x_j}\left[\left(\mu + \frac{\mu_\mathrm{t}}{\sigma_\mathrm{k}}\right)\frac{\partial k}{\partial x_j}\right] + G_\mathrm{k} - \rho\varepsilon \tag{4}$$

$$\frac{\partial(\rho\varepsilon)}{\partial t} + \frac{\partial(\rho\varepsilon u_i)}{\partial x_i} = \frac{\partial}{\partial x_j}\left[\left(\mu + \frac{\mu_t}{\sigma_\varepsilon}\right)\frac{\partial \varepsilon}{\partial x_j}\right] + \mathrm{C}_{1\varepsilon}\frac{\varepsilon}{k}G_\mathrm{k} - \mathrm{C}_{2\varepsilon}\frac{\rho\varepsilon^2}{k} \tag{5}$$

where k is the turbulence kinetic energy, m^2/s^2; ε is the dissipation rate; u_i is the speed vector, m/s; μ_t is the eddy viscosity, Pa·s; σ_k and σ_ε is the Turbulent Prandtl numbers; $\mathrm{C}_{1\varepsilon}$ and $\mathrm{C}_{2\varepsilon}$ are the model courants; and G_k is the generation of k due to mean velocity gradients.

2.3. Assumptions and Boundary Conditions

In this study, these assumptions were made to simplify the calculations: (1) air, both indoor and outdoor, was an ideal, incompressible gas; (2) air was thought of as a two-phase

mixture consisting of dry air and water vapor; (3) the weather outside was favorable; and (4) the wind direction was constant over the whole simulation range.

Furthermore, the simulation model's accuracy was somewhat impacted by the choice of experimental materials. The enclosure structure's thickness, density, specific heat, and thermal conductivity were what determined how well the greenhouse and corridor are insulated. The greenhouse effect intensity was directly influenced by the rate at which each surface absorbs radiation. The material parameters of the model in numerical calculations are shown in Table 1. The solar radiation value is calculated using Fluent's built-in solar calculator, with the geographical location set to 123.41° N, 41.3° E, and a time zone of GMT + 8. The coefficient of sunny days is 0.9.

Table 1. Material parameters in the simulation model.

Materials	Thickness, mm	Density, kg/m^3	Specific Heat Capacity, J/(kg·°C)	Thermal Conductivity, W/(m·°C)	Solar Radiation Absorption Rate, %	Solar Radiation Transmittance, %
Brick wall	370	1350	1062	0.58	0.9	—
Polystyrene board	110	30	1368	0.042	—	—
Wooden board	370	500	2520	0.29	0.7	—
Soil	—	1800	828	1.16	0.86	—
PO film	0.2	970	750	0.34	0.1	0.8
Heat preservation quilt	40	300	1275	0.11	0.01	—

2.4. Correctness Verification

The simulation model was validated by our research team in other studies [29,30]. The model selection, boundary conditions, material parameters, and solver settings of this model have not changed. Here, it was not reiterated.

3. Results and Discussion

The temperature distribution across the greenhouse and corridor surfaces is depicted in Figure 3. The solar greenhouse cluster's corridors have an unequal distribution of heat, which negatively affects the greenhouse's internal temperature distribution. To effectively control the temperature and humidity distribution in the corridor, this study simulated the structural parameters, ventilation techniques, wind speed, and direction of the corridor.

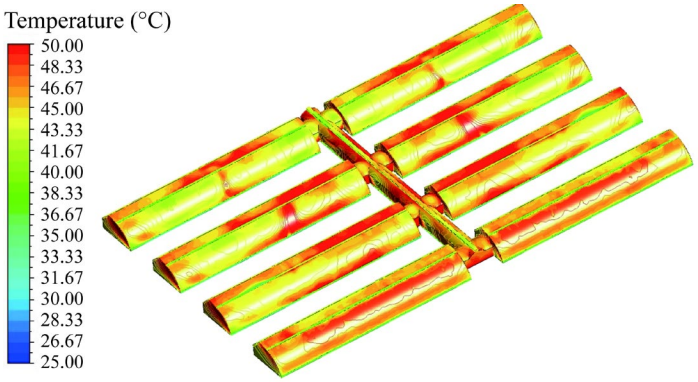

Figure 3. Temperature distribution of the corridor in the solar greenhouse cluster.

3.1. Effect of Corridor Structure on Ventilation Effect

3.1.1. Corridor Height

Figure 4a shows the internal temperature and humidity distribution of the corridor at different h. At this time, the width of the corridor is w = 5 m, and a combination of top and bottom ventilation is used. The corridor with h = 3.2 m has a lower temperature. The temperature rises gradually as h increases because the heated area in the corridor also increases significantly. The heated area's size is the primary indicator of how h affects

temperature. There are comparatively fewer heating zones and colder temperatures in the corridors at lower heights. Additionally, the location within the corridor has an impact on the temperature distribution. The southern end of the corridor and the second horizontal intersection on the south side of the corridor are the two positions where the temperature is higher. In addition, the temperature distribution inside the corridor is completely different from that on the surface. The high temperature on the surface of the corridor is concentrated on the north side of the corridor, and the high temperature inside is concentrated on the south side of the corridor. The humidity distribution in the corridors with various h is depicted in Figure 4b. At h = 3.2 m and h = 3.7 m, respectively, the humidity levels inside the corridor are the lowest and highest. Significant differences in humidity regulation are observed between corridors of varying heights. On the south windward side, there is a localized high humidity condition, and the quantity of air exchange in the corridor affects the water vapor content. Water vapor cannot be swiftly released due to the obstruction of the airflow on the south-windward side.

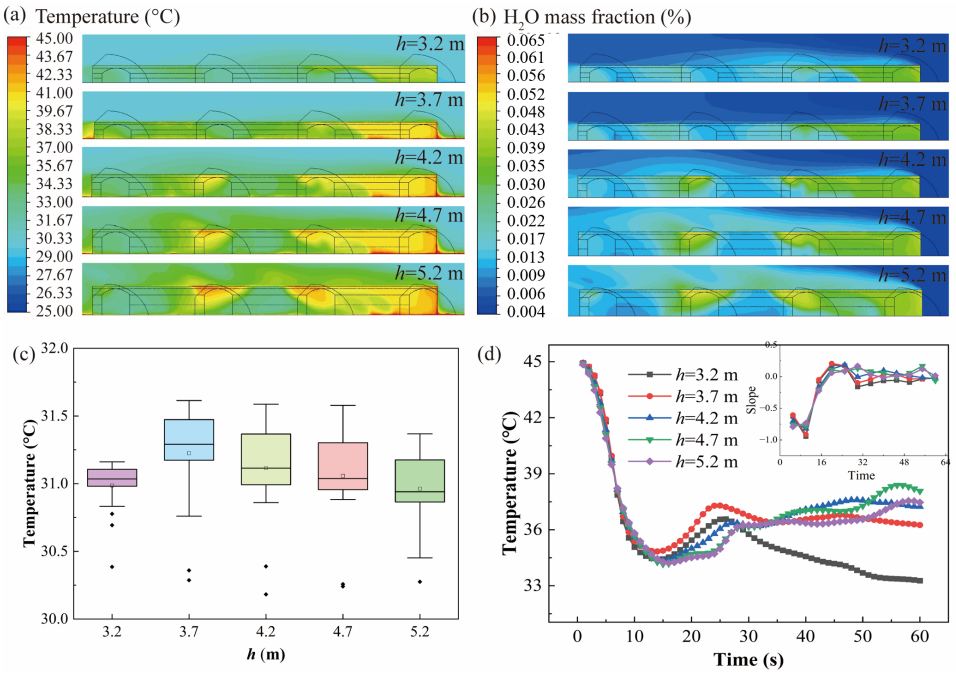

Figure 4. Influence of h on the corridor ventilation: (**a**) Temperature distribution; (**b**) Humidity distribution; (**c**) Temperature fluctuation; (**d**) Temperature variations with time.

The average temperature values of corridors with various h are displayed in Figure 4c. At h = 3.7 m, the corridor's temperature is noticeably higher than it is at other heights. Figure 4d shows that the corridor temperature increases more quickly after 15 s and then steadily stabilizes after 30 s at h = 3.7 m. In comparison to other corridor heights, the temperature rises most slowly and steadily at h = 5.2 m after 15 s. As a result, corridors with lower heights are more vulnerable to the greenhouse effect, which causes temperatures to rise more quickly between 15 and 25 s. When h = 5.2 m, the corridor height is close to the greenhouse height, and the temperature rise is slower. This phenomenon is caused by the fact that the optical thickness of the corridor decreases with height, increasing the amount of short-wave radiation absorbed by the walls and ground, which has a higher absorption rate. Both experience a faster rise in temperature, which results in more long-wave radiation being emitted and absorbed by greenhouse air. Convective heat transfer allows for a larger temperature differential between the air and its surface, which facilitates the easier extraction of energy. On the contrary, the rate of temperature rise is relatively small. But when h = 3.2 m, the final corridor temperature is lower, which is the goal pursued by corridor ventilation. It is worth noting that the average body temperature (Figure 4d) is higher than the average temperature obtained by sampling (Figure 4c). This is caused by

the discrete radiation model's high temperature on the corridor's semi-transparent surface, so a thorough examination of both is needed.

3.1.2. Corridor Width

At a height of h = 4.2 m, Figure 5a displays the temperature distribution of corridors with varying widths. A combination of top and bottom ventilation is used. The temperature is generally higher and varies greatly when w = 4 m. For the 5 and 6 m wide corridors, there are variations in the quantity of anomalous data points as well as in the stability of temperature data. The overall uniformity and temperature distribution are better in the 7 m corridor. From Figure 5b, during 0~10 s, the influence of corridor width on the temperature field is essentially the same. At different times, the influence of w on the temperature field exhibits distinct patterns. Corridors with varying widths may affect the temperature field similarly in short times, but certain widths of corridors may see minor or large temperature increases in particular times. A corridor of w = 5 m is the most appropriate, considering both the ventilation impact and construction cost.

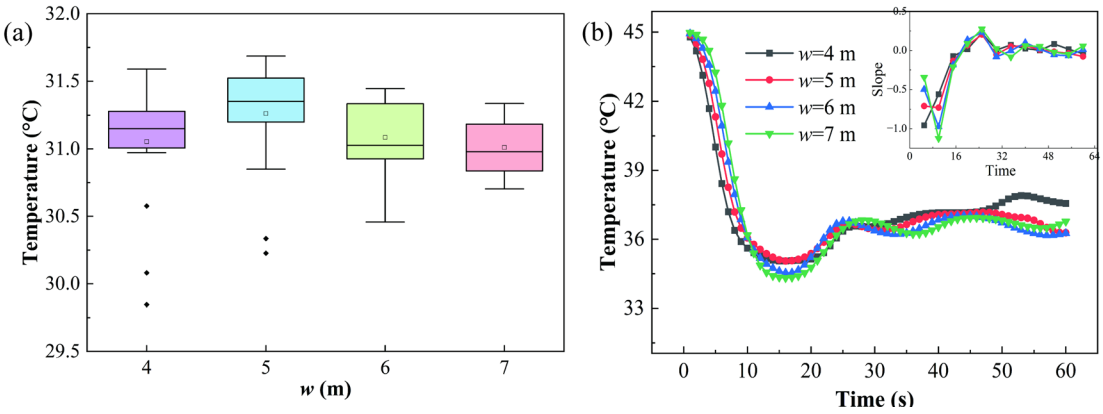

Figure 5. Influence of w on the corridor temperature: (**a**) Temperature fluctuation; (**b**) Temperature variations with time.

3.2. Effect of Corridor Window Openings on the Ventilation Effect

3.2.1. Distribution of Ventilation Openings

Figure 6 illustrates the impact of various window distributions on the corridor's temperature at h = 4.2 m and w = 5 m. It goes without saying that opening the top window alone has much less of a cooling effect than opening the bottom window alone and opening the top and bottom windows at the same time. Furthermore, the temperature drop rate is noticeably faster when the top and bottom windows are opened at the same time.

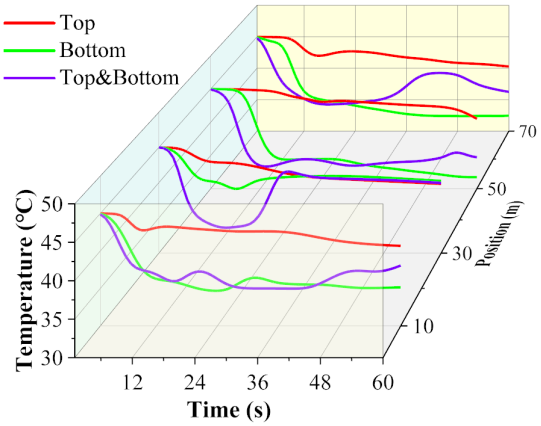

Figure 6. Temperature variations at different positions with different ventilation openings.

The corridor temperature and its variations over time under various ventilation methods are displayed in Figures 7a and 7b, respectively, to further compare their cooling effects. The average temperature determined at various points during a 40 s corridor ventilation period is displayed in Figure 7a. The corridor with only the top window open currently has the lowest and most consistent temperature. This may be because the hot air is effectively expelled from the corridor at this time. However, since this is an immediate effect, it does not follow that simply opening the top window for ventilation is preferable. The average temperature is highest but the temperature distribution within the corridor is more uniform when only the bottom window is open. Extremely low temperatures occur when the bottom and top windows are open at the same time, creating the most uneven temperature distribution in the corridor. This represents that the airflow inside the corridor is the most intense under this ventilation method.

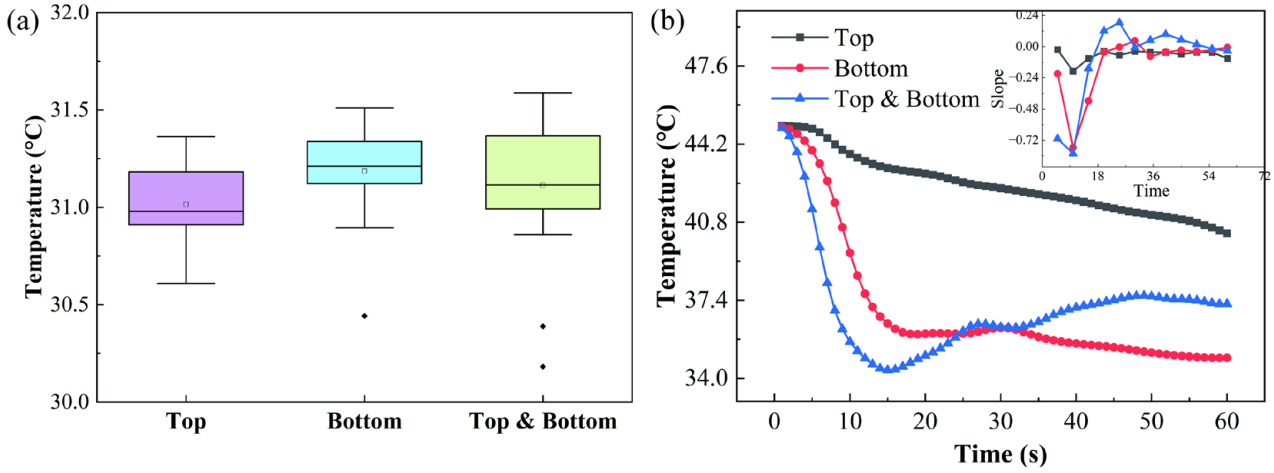

Figure 7. Influence of window distribution on corridor temperature: (**a**) Temperature fluctuation; (**b**) Temperature variations with time.

Figure 7b shows the trend of the average body temperature of the corridor over time under different ventilation methods. Compared to the other two methods, the top ventilation method has the slowest cooling rate. The ventilation effect of only opening the top window is poor and cannot effectively reduce the corridor temperature. Within the first 15 s, the cooling rate of combined ventilation is faster than that of bottom ventilation. When the bottom and top windows are opened simultaneously, it can lower the corridor temperature faster. However, combined ventilation may lead to temperature rise, while bottom ventilation may have a better cooling effect throughout the entire process. Therefore, when designing and managing corridors, it is necessary to comprehensively consider the characteristics of different window opening methods and choose appropriate ventilation strategies to achieve the best temperature regulation effect.

3.2.2. Thermal Ventilation and Chimney Effect

A reduction in indoor pressure results from the easier expulsion of hot air from the top ventilation window when both the top and bottom windows are open. However, it cannot be ensured that outdoor air will always enter the room through the bottom window because of the large scale of the corridor. Figure 8 illustrates the analysis of the airflow direction at the window for this purpose. The air in the bottom window primarily flows into the corridor, while the air in the top window primarily flows out of the corridor, according to the proportionate distribution of air flow velocity. This indicates that thermal ventilation and chimney effect are important influencing factors that cannot be ignored in the ventilation form where the top and bottom windows are opened simultaneously.

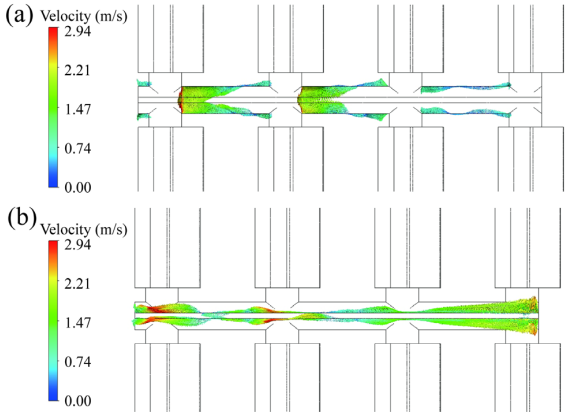

Figure 8. Airflow distribution at the corridor window: (**a**) Bottom window; (**b**) Top window.

3.2.3. Bottom Window Opening Ratio

As Figure 9a illustrates, the corridor temperature is also affected by the bottom window opening ratio η. The corridor's high-temperature zone and overall temperature are at their highest when η = 10%. In contrast, when η = 30%, 50% and 90%, the high-temperature area of the corridor decreases, and the highest temperature area usually occurs on the south side of the corridor. Therefore, a modest opening of the bottom window can lessen the area that experiences high temperatures, thereby lowering the corridor's temperature and increasing comfort. In general, the corridor's high-temperature region is the smallest and the temperature distribution is the most consistent when η = 70%. The impact of bottom window opening on corridor humidity is depicted in Figure 9b. The highest humidity is at η = 10%. There is little difference in humidity when η is 30%, 50%, 70%, and 90%. Figure 9c shows that, following 40 s of ventilation, the temperature is lower as the bottom window opening η is 10% and 90%. The temperature stabilizes and the data are most concentrated when η = 70%.

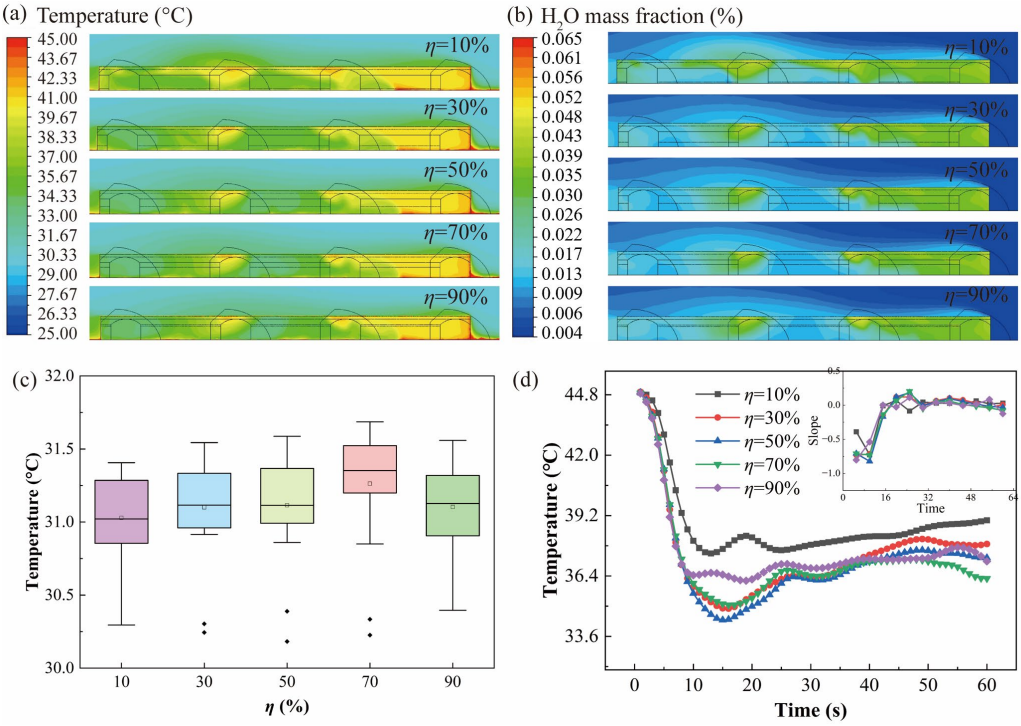

Figure 9. Influence of η on the corridor ventilation: (**a**) Temperature distribution; (**b**) Humidity distribution; (**c**) Temperature fluctuation; (**d**) Temperature variations with time.

As can be observed from Figure 9d, the temperature is high, the cooling threshold is at its smallest, and the fluctuations are significant when η = 10%. After 10 s of cooling, the temperature stops dropping when η = 90% and progressively gets closer to a steady state. This suggests that the temperature will not drop to its absolute minimum with excessive ventilation. When η = 30%, 50%, and 70%, the indoor temperature rebounds within 10 s to 30 s. After 30 s, the temperature tends to stabilize, with a lower temperature at η = 70%, indicating the best ventilation effect.

3.3. Effect of Wind Speed and Direction on the Ventilation Effect

3.3.1. Wind Speed

After determining the optimal parameters of the corridor structure (h = 3.2 m, w = 5 m) and the ventilation method (top ventilation + bottom ventilation, with η = 70%), this section analyzes the influence of wind speed and direction on the corridor's ventilation effect.

Figure 10 illustrates the temperature variations in the corridor under various wind speed conditions (1.5 m/s, 2 m/s, 2.5 m/s, 3 m/s, and 3.5 m/s) when the solar greenhouse cluster is exposed to a south wind. Lower wind speeds often achieve better cooling effects, with lower turbulence intensity at ventilation openings and more stable airflow. Higher wind speeds increase the flow speed of air, causing heat in the air to be carried away faster. But currently, the turbulence intensity of the airflow is high, and the indoor air flow is chaotic, which also easily leads to obstruction of air discharge. Overall, at low wind speeds, it is still possible to effectively reduce temperature through air flow and achieve good cooling effects.

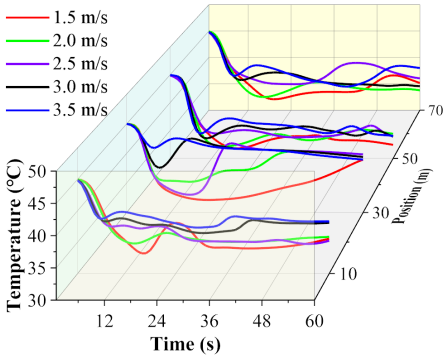

Figure 10. Variations in temperature over time at different positions of the corridor with varying wind speeds.

3.3.2. Wind Direction

Figure 11a illustrates how the temperature inside the corridor exhibits a specific trend as the wind direction gradually varies from the east to the south. When the east and west winds are blowing downward, the temperature inside the corridor is lower and the data distribution is more concentrated. The optimal ventilation effect is achieved at this point because the airflow is perpendicular to the corridor opening and passes straight through it. When the south wind is blowing downward, the temperature is the highest. The airflow is parallel to the corridor's windows, making it difficult for air to enter the corridor. It is evident from Figure 11b that the trend of temperature variations varies with wind direction. The trends of the west and east directions almost overlap, suggesting that these two directions influence temperature regulation in a comparable way. After 10 s, the decline stops and experiences a brief rebound before continuing to decline again, gradually increasing after 40 s. The wind direction has a symmetrical effect on corridor ventilation. The greater the velocity component of the airflow perpendicular to the window, the more beneficial the ventilation is [31].

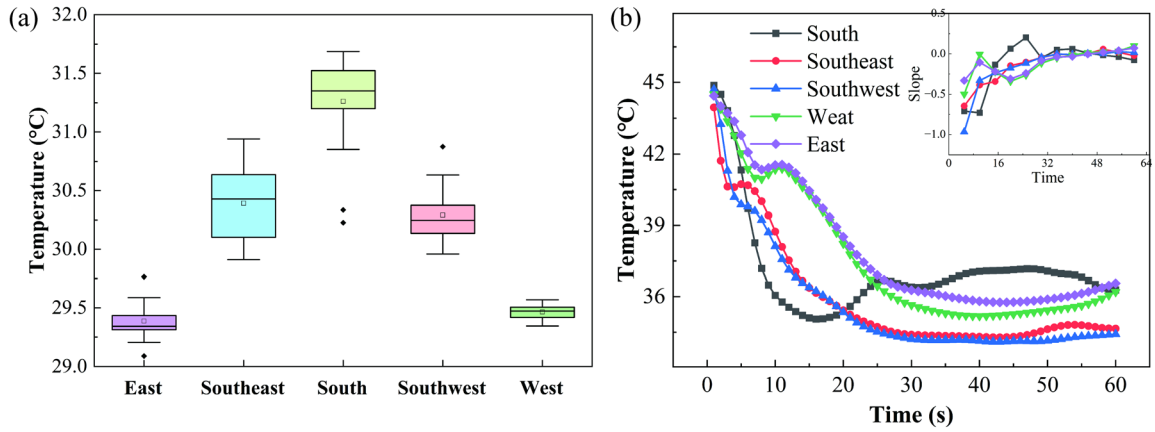

Figure 11. Influence of wind direction on corridor temperature: (**a**) Temperature fluctuation range; (**b**) Temperature change over time.

4. Conclusions

(1) A mechanized corridor is beneficial for improving the efficiency of solar greenhouse clusters, but there may be a phenomenon of concentrated heat distribution. Following a thorough analysis for ventilation, 3.2 m in height and 5 m in width is the optimal structure for the corridor;

(2) Bottom + top ventilation, with a 70% bottom window opening ratio, is the optimal ventilation strategy for the modern solar greenhouse corridor. The combined ventilation method achieves more efficient airflow in the corridor and effectively reduces the corridor temperature;

(3) The optimal wind speed for the external corridor of a modern solar greenhouse cluster is 2 m/s, and the optimal wind directions are east and west. The ventilation effect is significantly enhanced by this wind speed and direction.

Author Contributions: M.H. and X.J. contributed equally to this work; Conceptualization, M.H.; Methodology, X.J.; Theoretical calculations, M.H.; Formal analysis, X.W.; Investigation, Y.L.; Data curation, X.J.; Writing—original draft preparation, M.H. and X.W.; Writing—review and editing, M.H. and X.L.; Supervision, Q.F. and X.L.; Project administration, Q.F. All authors have read and agreed to the published version of the manuscript.

Funding: This work was funded by the Liaoning Provincial Natural Science Foundation Program (2024-BS-085), the "Open Competition Mechanism to Select the Best Candidates" Program in the Xinjiang Production and Construction Crops (2022AA003), and the China Agricultural Research System, China (CARS-23).

Data Availability Statement: Dataset available upon request from the authors.

Conflicts of Interest: The authors declare no conflicts of interest.

References

1. Ismail, M.M.; Dincer, I.; Bicer, Y.; Saghir, M.Z. Effect of using phase change materials on thermal performance of passive solar greenhouses in cold climates. *Int. J. Thermofluids* **2023**, *19*, 100380. [CrossRef]
2. Nicholas, K.; Stanley, P.D.; Joshua, W.; San, C.; Denis, M.; Emmanuel, Z.; Faizal, M.; Alessandra, F. Greenhouse gas emissions from Uganda's cattle corridor farming systems. *Agric. Syst.* **2019**, *176*, 102649.
3. Li, Y.R.; Jian, Y.B.; Wang, S.; Liu, X.; Li, W.X.; Arici, M.; Zhang, L.L.; Li, W.L.; Cao, Y. Spatial temperature distribution and ground thermal storage in the plastic greenhouse: An experimental and modeling study. *J. Energy Storage* **2024**, *77*, 109938. [CrossRef]
4. Boulard, T.; Wang, S. Experimental and numerical studies on the heterogeneity of crop transpiration in a plastic tunnel. *Comput. Electron. Agric.* **2002**, *34*, 173–190. [CrossRef]
5. Bartzanas, T.; Boulard, T.; Kittas, C. Effect of vent arrangement on windward ventilation of a tunnel greenhouse. *Biosyst. Eng.* **2004**, *88*, 479–490. [CrossRef]
6. Abbes, M.; Farhat, A.; Mami, A.; Dauphin-Tanguy, G. Pseudo bond graph model of coupled heat and mass transfers in a plastic tunnel greenhouse. *Simul. Model. Pract. Theory* **2010**, *18*, 1327–1341. [CrossRef]

7. He, Z.H.; Su, C.J.; Cai, Z.L.; Wang, Z.; Li, R.; Liu, J.C.; He, J.Q.; Zhang, Z. Multi-factor coupling regulation of greenhouse environment based on comprehensive growth of cherry tomato seedlings. *Sci. Hortic-Amst.* **2022**, *297*, 110960. [CrossRef]
8. Li, L.; Li, H.T.; Liu, N.; Lu, Y.; Shao, L.W.; Chen, S.Y.; Zhang, X.Y. Water use characteristics and drought tolerant ability of different winter wheat cultivars assessed under whole growth circle and at seedling stage. *Agric. Water Manag.* **2024**, *300*, 108921. [CrossRef]
9. Feng, J.Y.; Hu, X.P. An IoT-based hierarchical control method for greenhouse seedling production. *Procedia Comput. Sci.* **2021**, *192*, 1954–1963. [CrossRef]
10. Morad, M.M.; El-Shazly, M.A.; Wasfy, K.I.; El-Maghawry Hend, A.M. Thermal analysis and performance evaluation of a solar tunnel greenhouse dryer for drying peppermint plants. *Renew. Energy* **2017**, *101*, 992–1004. [CrossRef]
11. Patil, R.; Gawande, R. A review on solar tunnel greenhouse drying system. *Renew. Sust. Energy Rev.* **2016**, *56*, 196–214. [CrossRef]
12. Duraivel, B.; Muthuswamy, N.; Gnanavendan, S. Comprehensive analysis of the greenhouse solar tunnel dryer (GSTD) using Tomato, snake Gourd, and Cucumber: Insights into energy Efficiency, exergy Performance, economic Viability, and environmental impact. *Sol. Energy* **2024**, *267*, 112263. [CrossRef]
13. Condori, M.; Echazu, R.; Saravia, L. Solar drying of sweet pepper and garlic using the tunnel greenhouse drier. *Renew. Energy* **2001**, *22*, 447–460. [CrossRef]
14. Ding, G.Q.; Yi, D.; Yi, J.L.; Guo, J.; Ou, M.H.; Ou, W.X.; Tao, Y.; Pueppke, S.G. Protecting and constructing ecological corridors for biodiversity conservation: A framework that integrates landscape similarity assessment. *Appl. Geogr.* **2023**, *160*, 103098. [CrossRef]
15. Zhao, Y.; Ko, J. Vocational teachers' perceptions on workplace learning in facilitating students' professional engagement in the context of industry-university collaboration in China. *J. Workplace Learn.* **2024**, *36*, 282–297. [CrossRef]
16. He, X.L.; Wang, J.; Guo, S.R.; Zhang, J.; Wei, B.; Sun, J.; Shu, S. Ventilation optimization of solar greenhouse with removable back walls based on CFD. *Comput. Electron. Agric.* **2018**, *149*, 16–25. [CrossRef]
17. Fu, W.H.; You, S.J. The numerical simulation of thermal environment strawberry greenhouse in natural ventilation. *Appl. Mech. Mater.* **2014**, *501–504*, 2276–2281. [CrossRef]
18. Zhang, G.X.; Fu, Z.T.; Yang, M.S.; Liu, X.X.; Dong, Y.H.; Li, X.X. Nonlinear simulation for coupling modeling of air humidity and vent opening in Chinese solar greenhouse based on CFD. *Comput. Electron. Agric.* **2019**, *162*, 337–347. [CrossRef]
19. Li, H.; Li, Y.M.; Yue, X.; Liu, X.A.; Tian, S.B.; Li, T.L. Evaluation of airflow pattern and thermal behavior of the arched greenhouses with designed roof ventilation scenarios using CFD simulation. *PLoS ONE* **2020**, *15*, e0239851. [CrossRef]
20. Zhang, L.; Liu, X.A.; Shi, W.B.; Li, T.L.; Ji, J.W. Study of a novel front-roof-back natural ventilation system for Chinese solar greenhouses. *Roy. Soc. Open Sci.* **2022**, *9*, 220251. [CrossRef]
21. Schatzmann, M.; Leitl, B. Issues with validation of urban flow and dispersion CFD models. *J. Wind Eng. Ind. Aerodyn.* **2011**, *99*, 169–186. [CrossRef]
22. Jiang, Z.W.; Cheng, H.M.; Zhang, P.H.; Kang, T.F. Influence of urban morphological parameters on the distribution and diffusion of air pollutants: A case study in China. *J. Environ. Sci.* **2021**, *105*, 163–172. [CrossRef] [PubMed]
23. Zhou, H.; Lu, Y.J.; Liu, X.D.; Chang, R.D.; Wang, B. Harvesting wind energy in low-rise residential buildings: Design and optimization of building forms. *J. Clean. Prod.* **2017**, *167*, 306–316. [CrossRef]
24. Argento, S.; Garcia, G.; Treccarichi, S. Sustainable and low-input techniques in Mediterranean greenhouse vegetable production. *Horticulturae* **2024**, *10*, 997. [CrossRef]
25. Sousa, P.; Rodrigues, C.V.; Afonso, A. Enhancing CFD solver with Machine Learning techniques. *Comput. Methods Appl. Mech. Eng.* **2024**, *429*, 11713. [CrossRef]
26. Wang, J.B.; Zeng, L.C.; Fu, T.; Yu, S.; He, Y.T. Effects of the position and perforation parameters of the delta winglet vortex generators on flow and heat transfer in minichannels. *Int. J. Therm. Sci.* **2024**, *198*, 108878. [CrossRef]
27. Kang, L.Y.; Zhang, Y.; Kacira, M.; van Hooff, T. CFD simulation of air distributions in a small multi-layer vertical farm: Impact of computational and physical parameters. *Biosyst. Eng.* **2024**, *243*, 148–174. [CrossRef]
28. Lateb, M.; Masson, C.; Stathopoulos, T.; Bedard, C. Comparison of various types of k–ε models for pollutant emissions around a two-building configuration. *J. Wind Eng. Ind. Aerodyn.* **2013**, *115*, 9–21. [CrossRef]
29. Fan, Z.L.; Li, Y.M.; Jiang, L.L.; Wang, L.; Li, T.L.; Liu, X.A. Analysis of the effect of exhaust configuration and shape parameters of ventilation windows on microclimate in round arch solar greenhouse. *Sustainability* **2023**, *15*, 6432. [CrossRef]
30. Li, H.; Ji, D.; Hu, X.; Xie, T.; Song, W.T.; Tian, S.B. Comprehensive evaluation of combining CFD simulation and entropy weight to predict natural ventilation strategy in a sliding cover solar greenhouse. *Int. J. Agric. Biol. Eng.* **2021**, *14*, 213–221. [CrossRef]
31. Hu, H.; Kikumoto, H.; Ooka, R. Effect of wind direction on natural ventilation in a multiple-room house via field measurements and numerical simulations. *J. Wind Eng. Ind. Aerodyn.* **2024**, *248*, 105718. [CrossRef]